

HIGHER AND MISSING RESONANCES IN ω PHOTOPRODUCTION

YONGSEOK OH

Institute of Physics and Applied Physics, Yonsei University, Seoul 120-749, Korea
E-mail: yoh@phya.yonsei.ac.kr

ALEXANDER I. TITOV

Bogoliubov Laboratory of Theoretical Physics, JINR, Dubna 141980, Russia
E-mail: atitov@thsun1.jinr.ru

T.-S. H. LEE

Physics Division, Argonne National Laboratory, Argonne, Illinois 60439, U.S.A.
E-mail: lee@theory.phy.anl.gov

We study the role of the nucleon resonances (N^*) in ω photoproduction by using the quark model resonance parameters predicted by Capstick and Roberts. The employed $\gamma N \rightarrow N^*$ and $N^* \rightarrow \omega N$ amplitudes include the configuration mixing effects due to the residual quark-quark interactions. The contributions from the nucleon resonances are found to be important in the differential cross sections at large scattering angles and various spin observables. In particular, the parity asymmetry and beam-target double asymmetry at forward scattering angles are suggested for a crucial test of our predictions. The dominant contributions are found to be from $N_{\frac{3}{2}}^3(1910)$, a missing resonance, and $N_{\frac{3}{2}}^3(1960)$ which is identified as the $D_{13}(2080)$ of the Particle Data Group.

The nucleon resonances predicted by the constituent quark models have a much richer spectrum than what have been observed in pion-nucleon scattering¹. The origin of this “missing resonance problem” has been ascribed to the possibility that many predicted nucleon resonances (N^*) could couple weakly to the πN channel². Therefore it would be legitimate to study the nucleon resonances in other reactions and vector meson electromagnetic production is one of them which are under investigation at current experimental facilities such as TJNAF, ELSA-SAPHIR, GRAAL, and LEPS of SPring-8. Theoretically the role of the nucleon resonances was studied by Zhao *et al.*^{3,4} based on an effective Lagrangian method within the $SU(6) \times O(3)$ constituent quark model.

Our study on the nucleon resonances in vector meson photoproduction⁵ is based on the quark model predictions by Capstick and Roberts⁶, where the configuration mixing effects due to the residual quark-quark interactions are included and the hadron decays are calculated by using the 3P_0 model. The

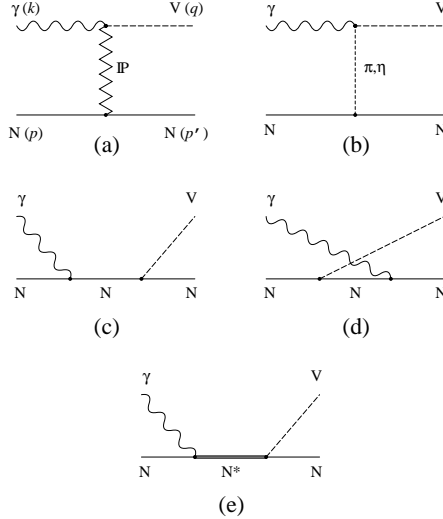


Figure 1. Diagrammatic representation of ω photoproduction mechanisms: (a) Pomeron exchange, (b) (π, η) exchange, (c) direct nucleon term, (d) crossed nucleon term, and (e) s -channel nucleon excitations.

predicted baryon wave functions and the N^* decay amplitudes are considerably different from those of the $SU(6) \times O(3)$ quark model³. Thus it would be interesting to find the differences in the model predictions on vector meson photoproduction, which can be tested experimentally.

In this work we focus on ω photoproduction⁵ since its non-resonant reaction mechanisms are rather well understood and the isosinglet nature of the ω meson allows the contributions from the isospin-1/2 nucleon resonances only. Earlier studies on ω photoproduction⁷ show that the reaction is dominated by diffractive processes at high energies, i.e., via the Pomeron exchange, and by one-pion exchange at low energies. It is therefore reasonable to follow the earlier theoretical analyses and assume that the non-resonant amplitude of ω photoproduction can be calculated from these two well-established mechanisms with some refinements. The resulting model then can be a starting point for investigating the N^* effects.

Our model for ω photoproduction, therefore, can be described by the diagrams shown in Fig. 1. The Pomeron exchange [Fig. 1(a)] is known to govern the total cross sections and differential cross sections at low $|t|$ in the high energy region for electromagnetic production of vector mesons. For this

model, we follow the Donnachie-Landshoff model⁸. The details on this model can be found, e.g., in Refs.^{9,10} and the resulting amplitude and the parameters are summarized in Refs.^{5,11}.

The pseudoscalar meson exchange amplitudes [Fig. 1(b)] are calculated from the following effective Lagrangians:

$$\begin{aligned}\mathcal{L}_{\omega\gamma\varphi} &= \frac{eg_{\omega\gamma\varphi}}{M_V} \epsilon^{\mu\nu\alpha\beta} \partial_\mu \omega_\nu \partial_\alpha A_\beta \varphi, \\ \mathcal{L}_{\varphi NN} &= -ig_{\pi NN} \bar{N} \gamma_5 \tau_3 N \pi^0 - ig_{\eta NN} \bar{N} \gamma_5 N \eta,\end{aligned}\quad (1)$$

where $\varphi = (\pi^0, \eta)$ and A_β is the photon field. We use $g_{\pi NN}^2/4\pi = 14$ and $g_{\eta NN}^2/4\pi = 0.99$ for the πNN and ηNN coupling constants, respectively. The coupling constants $g_{\omega\gamma\varphi}$ can be estimated through the decay widths of $\omega \rightarrow \gamma\pi$ and $\omega \rightarrow \gamma\eta$ ¹² which lead to $g_{\omega\gamma\pi} = 1.823$ and $g_{\omega\gamma\eta} = 0.416$. The higher mass of the η and the associated small coupling constants suppress the η exchange contribution compared with the π exchange. The φNN and $\omega\gamma\varphi$ vertices are dressed by the form factors,

$$F_{\varphi NN}(t) = \frac{\Lambda_\varphi^2 - M_\varphi^2}{\Lambda_\varphi^2 - t}, \quad F_{\omega\gamma\varphi}(t) = \frac{\Lambda_{\omega\gamma\varphi}^2 - M_\varphi^2}{\Lambda_{\omega\gamma\varphi}^2 - t}, \quad (2)$$

with $\Lambda_\pi = 0.6$ GeV and $\Lambda_{\omega\gamma\pi} = 0.7$ GeV⁵, $\Lambda_\eta = 1.0$ GeV and $\Lambda_{\omega\gamma\eta} = 0.9$ GeV¹³.

The nucleon pole terms [Fig. 1(c,d)] are calculated from the following interaction Lagrangians:

$$\begin{aligned}\mathcal{L}_{\gamma NN} &= -e\bar{N} \left(\gamma_\mu \frac{1+\tau_3}{2} A^\mu - \frac{\kappa_N}{2M_N} \sigma^{\mu\nu} \partial_\nu A_\mu \right) N, \\ \mathcal{L}_{\omega NN} &= -g_{\omega NN} \bar{N} \left(\gamma_\mu \omega^\mu - \frac{\kappa_\omega}{2M_N} \sigma^{\mu\nu} \partial_\nu \omega_\mu \right) N,\end{aligned}\quad (3)$$

with the anomalous magnetic moment of the nucleon $\kappa_{p(n)} = 1.79$ (-1.91). For the coupling constants we use $g_{\omega NN} = 10.35$ and $\kappa_\omega = 0$ ^{14,15}. In order to dress the vertices, we include the form factor¹⁶,

$$F_N(r) = \frac{\Lambda_N^4}{\Lambda_N^4 - (r - M_N^2)^2}, \quad (4)$$

where $r = s$ or t and $\Lambda_N = 0.5$ GeV.

With the non-resonant amplitudes discussed above we estimate the nucleon resonance contributions by making use of the quark model predictions⁶ on the resonance photoexcitation $\gamma N \rightarrow N^*$ and the resonance decay $N^* \rightarrow N\omega$. In this work we consider the s -channel diagrams shown in Fig. 1(e).

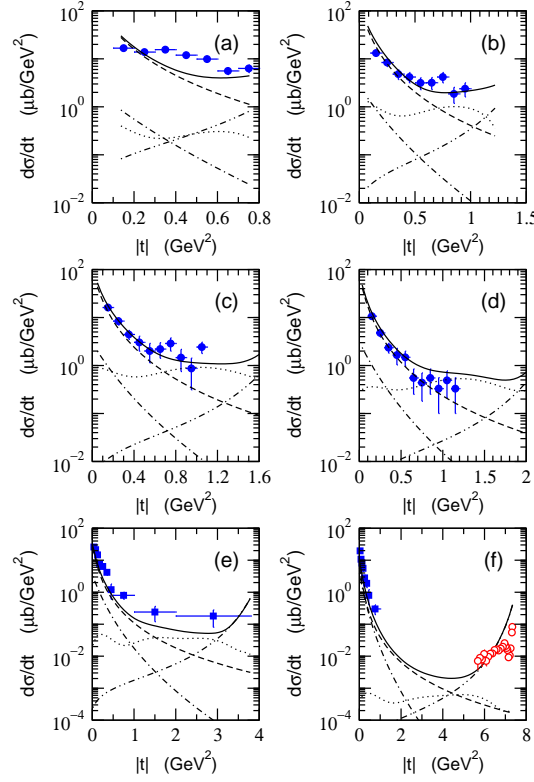


Figure 2. Differential cross sections for $\gamma p \rightarrow p\omega$ reaction as a function of $|t|$ at $E_\gamma =$ (a) 1.23, (b) 1.45, (c) 1.68, (d) 1.92, (e) 2.8, and (f) 4.7 GeV. The results are from pseudoscalar-meson exchange (dashed), Pomeron exchange (dot-dashed), direct and crossed nucleon terms (dot-dot-dashed), N^* excitation (dotted), and the full amplitude (solid). Data are taken from Ref. ¹⁷ [filled circles in (a,b,c,d)], Ref. ¹⁸ [filled squares in (e,f)], and Ref. ¹⁹ [open circles in (f)].

The crossed diagrams cannot be calculated from the informations available in Ref. ⁶. The resonant amplitude in the center of mass frame is written as

$$I_{m_f, m_\omega, m_i, \lambda_\gamma}^{N^*}(\mathbf{q}, \mathbf{k}) = \sum_{J, M_J} \frac{1}{\sqrt{s} - M_R^J + \frac{i}{2}\Gamma^J(s)} \mathcal{M}_{N^* \rightarrow N'\omega}(\mathbf{q}; m_f, m_\omega; J, M_J) \times \mathcal{M}_{\gamma N \rightarrow N^*}(\mathbf{k}; m_i, \lambda_\gamma; J, M_J), \quad (5)$$

where M_R^J is the N^* mass of spin quantum numbers (J, M_J) , and m_i, m_f, λ_γ ,

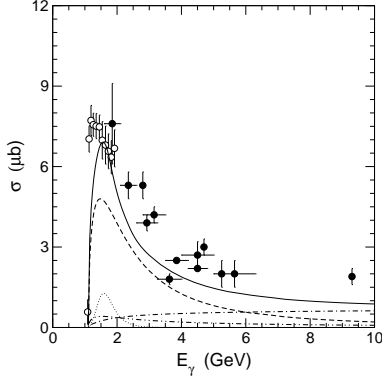


Figure 3. Total cross section of ω photoproduction. The notations are the same as in Fig. 2. Data are taken from Refs. 17,18,20.

and m_ω are the spin projections of the initial nucleon, final nucleon, incoming photon, and outgoing ω meson, respectively. In this study, we consider 12 positive parity and 10 negative parity nucleon resonances up to spin-9/2. The explicit form of the resonant amplitude and the details on the calculations can be found in Ref. 5 as well as the considered nucleon resonances and their parameters.

Our results for the differential cross section are shown in Fig. 2, which shows that the data can be described to a very large extent in the considered energy region, $E_\gamma \leq 5$ GeV. It is clear that the contributions due to the N^* excitations (dotted curves) and the direct and crossed nucleon terms (dot-dot-dashed curves) help bring the agreement with the data at large angles. The forward angle cross sections are mainly due to the interplay between the pseudoscalar-meson exchange (dashed curves) and the Pomeron exchange (dot-dashed curves). The main problem here is in reproducing the data at $E_\gamma = 1.23$ GeV. This perhaps indicates that the off-shell contributions from N^* 's below ωN threshold are important at very low energies.

The contribution from the nucleon resonances to total cross sections is shown in Fig. 3. To have a better understanding of the resonance contributions, we compare the contributions from the considered N^* 's to the differential and total cross sections. We found that the contributions from $N_{\frac{3}{2}}^3(1910)$ and $N_{\frac{3}{2}}^3(1960)$ are the largest at all energies up to $E_\gamma = 3$ GeV. The $N_{\frac{3}{2}}^3(1910)$ is a missing resonance, while $N_{\frac{3}{2}}^3(1960)$ is identified as a two star resonance $D_{13}(2080)$ of the Particle Data Group¹². This result

is significantly different from the quark model calculations of Ref. ³. The difference between the two calculations is not surprising since the employed quark models are rather different. In particular, our predictions include the configuration mixing effects due to residual quark-quark interactions. The discrepancy of our prediction with the experimental data at very low energy is again expected to be due to the nucleon resonances below ωN threshold, which are missed in our calculation.

Instead of the cross sections, the polarization asymmetries²¹ provide more appropriate tools to investigate the role of the nucleon resonances in ω photoproduction⁵. We first examined the single spin asymmetries⁵. Although our predictions are significantly different from those of Ref. ³, we confirm their conclusion that those asymmetries are sensitive to the nucleon resonances but mostly at large $|t|$ region.

More clear signal for the nucleon resonances can be found from the parity asymmetry (or photon polarization asymmetry) and the beam-target double asymmetry. These asymmetries are sensitive to the N^* contributions at forward angles, where precise measurements might be more favorable because the cross sections are peaked at $\theta = 0$. The parity asymmetry is defined as²²

$$P_\sigma = \frac{d\sigma^N - d\sigma^U}{d\sigma^N + d\sigma^U} = 2\rho_{1-1}^1 - \rho_{00}^1, \quad (6)$$

where σ^N and σ^U are the cross sections due to the natural and unnatural parity exchanges respectively, and $\rho_{\lambda,\lambda'}^i$ are the vector-meson spin density matrices. The beam-target double asymmetry is defined as²¹

$$C_{zz}^{BT} = \frac{d\sigma(\uparrow\downarrow) - d\sigma(\uparrow\uparrow)}{d\sigma(\uparrow\downarrow) + d\sigma(\uparrow\uparrow)}, \quad (7)$$

where the arrows represent the helicities of the incoming photon and the target proton. In Fig. 4, we show the results from calculations with (solid curves) and without (dotted curves) including N^* contributions. The difference between them is striking and can be unambiguously tested experimentally. Here we also find that the $N_{\frac{3}{2}}^3(1910)$ and $N_{\frac{3}{2}}^3(1960)$ are dominant. By keeping only these two resonances in calculating the resonant part of the amplitude, we obtain dashed curves which are not too different from the full calculations (solid curves).

To summarize, we investigated the role of the nucleon resonances in ω photoproduction. We found that the inclusion of the resonance amplitudes leads to a better description of the observed total and differential cross sections. It is also found that the $N_{\frac{3}{2}}^3(1910)$ and $N_{\frac{3}{2}}^3(1960)$ are dominant in the resonance amplitudes. As a further study on the nucleon resonances, we

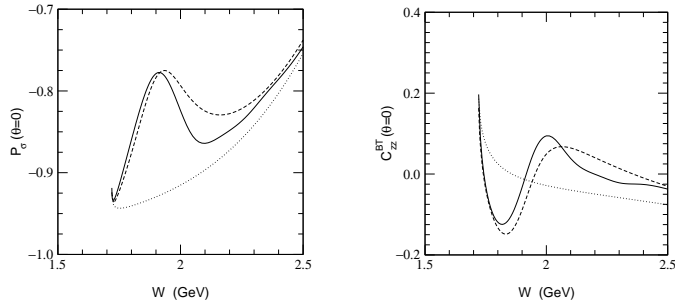


Figure 4. Parity asymmetry P_σ and beam-target double asymmetry C_{zz}^{BT} at $\theta = 0$ as functions of W . The dotted curves are calculated without including N^* effects, the dashed curves include contributions of $N_{\frac{3}{2}}^3(1910)$ and $N_{\frac{3}{2}}^3(1960)$ only, and the solid curves are calculated with all N^* 's up to spin-9/2.

suggest to measure the parity asymmetry and beam-target double asymmetry. Experimental test of our predictions will be a useful step toward resolving the so-called ‘‘missing resonance problem’’ or distinguishing different quark model predictions and could be done at current electron/photon facilities. Theoretically the predictions should be improved further. For example, the form factor of the vertices including the nucleon resonances should be studied in detail in the given quark models and the crossed N^* terms as well as the nucleon resonances below ωN threshold should be studied. Finally, the effects due to the initial and final state interactions must be also investigated especially at low energies.

Acknowledgments

This work was supported in part by the Brain Korea 21 project of Korean Ministry of Education, the International Collaboration Program of KOSEF under Grant No. 200006-111-01-2, Russian Foundation for Basic Research under Grant No. 96-15-96426, and U.S. DOE Nuclear Physics Division Contract No. W-31-109-ENG-38.

References

1. N. Isgur and G. Karl, Phys. Lett. **72B**, 109 (1977); Phys. Rev. D **18**, 4187 (1978); **19**, 2653 (1979), **23**, 817(E) (1981); R. Koniuk and N. Isgur, *ibid.* **21**, 1868 (1980).

2. See, e.g., S. Capstick and W. Roberts, nucl-th/0008028.
3. Q. Zhao, Z. Li, and C. Bennhold, Phys. Rev. C **58**, 2393 (1998); Q. Zhao, Phys. Rev. C **63**, 025203 (2001).
4. Q. Zhao, in these proceedings.
5. Y. Oh, A. I. Titov, and T.-S. H. Lee, Phys. Rev. C **63**, 025201 (2001); talk at SPIN 2000 Symposium, nucl-th/0012012.
6. S. Capstick, Phys. Rev. D **46**, 2864 (1992); S. Capstick and W. Roberts, *ibid.* **49**, 4570 (1994).
7. ABBHHM Collaboration, R. Erbe *et al.*, Phys. Rev. **175**, 1669 (1968); K. Schilling and F. Storim, Nucl. Phys. **B7**, 559 (1968); H. Fraas, *ibid.* **B36**, 191 (1972); J. Ballam *et al.*, Phys. Rev. D **7**, 3150 (1973); P. Joos *et al.*, Nucl. Phys. **B122**, 365 (1977); B. Friman and M. Soyeur, *ibid.* **A600**, 477 (1996).
8. A. Donnachie and P. V. Landshoff, Nucl. Phys. **B244**, 322 (1984); **B267**, 690 (1986); Phys. Lett. B **185**, 403 (1987); **296**, 227 (1992).
9. J.-M. Laget and R. Mendez-Galain, Nucl. Phys. **A581**, 397 (1995).
10. M. A. Pichowsky and T.-S. H. Lee, Phys. Rev. D **56**, 1644 (1997).
11. Y. Oh, A. I. Titov, and T.-S. H. Lee, talk at NSTAR 2000 Workshop, nucl-th/0004055.
12. Particle Data Group, D. E. Groom *et al.*, Eur. Phys. Jour. C **15**, 1 (2000).
13. A. I. Titov, T.-S. H. Lee, H. Toki, and O. Streltsova, Phys. Rev. C **60**, 035205 (1999).
14. T. Sato and T.-S. H. Lee, Phys. Rev. C **54**, 2660 (1996).
15. Th. A. Rijken, V. G. J. Stoks, and Y. Yamamoto, Phys. Rev. C **59**, 21 (1999).
16. H. Haberzettl, C. Bennhold, T. Mart, and T. Feuster, Phys. Rev. C **58**, 40 (1998).
17. F. J. Klein, Ph.D. thesis, Bonn Univ. (1996); SAPHIR Collaboration, F. J. Klein *et al.*, π N Newslett. **14**, 141 (1998).
18. J. Ballam *et al.*, Phys. Rev. D **7**, 3150 (1973).
19. R. W. Clifft *et al.*, Phys. Lett. **72B**, 144 (1977).
20. J. Ballam *et al.*, Phys. Lett. **30B**, 421 (1969); AHHM Collaboration, W. Struczinski *et al.*, Nucl. Phys. **B108**, 45 (1976); D. P. Barber *et al.*, Z. Phys. C **26**, 343 (1984).
21. A. I. Titov, Y. Oh, S. N. Yang, and T. Morii, Phys. Rev. C **58**, 2429 (1998).
22. K. Schilling, P. Seyboth, and G. Wolf, Nucl. Phys. **B15**, 397 (1970).